RESEARCH ON THE CRITICAL SIZE OF LIVE WORKING ROBOTS BETWEEN BUSBARS IN 220 kV SUBSTATIONS

Changsheng WU[1], Ji TIAN[2], Ronghuan MAI[3], Qiaoyun XU[4], Xianqiang LI[5]

Adopting live working robots to carry out live working can improve the safety of operators, which is especially true when performing live working in substations. This paper focus on the lowest discharge position and the critical size of live working robots between busbars under switching impulse. Finite element method (FEM) was used to calculate the electroquasistatic field. Based on the process of streamer and leader, the breakdown voltage of the phase-to-phase gap containing a robot is calculated. Between the busbars of 220 kV substations, the presented research shows that the lowest discharge position of live working robots locates in 61.5% of the phase-to-phase gap. Breakdown develops from d_1 gap once d_1 gap is less than 1.5 m. Moreover, presence of the live working robot results in a sharp drop to the breakdown voltage of the complex gap. Referring to the switching over-voltage and the risk of failure, the robot size should be designed less than 0.4 m for 220 kV substations.

Keywords: substation, live working, electric field, complex gap

1. Introduction

Discharge in long air gaps has been studied for over a century, that has been of crucial significance for electrical maintenance [1]. Especially when it comes to live working, which means working on the live equipment, adequate insulation gap must be ensured. Live working is an important way to improve the reliability of power supply [2]. It has been undertaken in power system for several decades.

As early as 1968, Armstrong and Whitehead [3, 4] established an electro-geometric model, which was based on the characteristic of negative polarity discharge. It may explain the flashover caused by lightning theoretically. Over the next decade or so, a lot of experiments were carried out. Gallimberti [5] in 1979 showed the process and mechanism of long spark formation. It was summarized that the spark formation developed through corona, streamer, leader and final

[1] Eng., Jiangmen Power Supply Bureau Co., Ltd., China, e-mail: cfwcs@163.com
[2] M.E, School of Automation, Wuhan University of Technology, China, e-mail: tianji@whut.edu.cn
[3] Eng., Jiangmen Power Supply Bureau Co., Ltd., China, e-mail: 88192936@qq.com
[4] Eng., Jiangmen Power Supply Bureau Co., Ltd., China, e-mail: 969380164@qq.com
[5] PhD Eng., School of Automation, Wuhan University of Technology, China, e-mail: lxq@whut.edu.cn

jump. In the late 1980s, Eriksson [6], Dellera [7, 8] and Rizk [9-12] proposed different models for leader propagation. These mathematical models are empirical or semi-empirical models based on discharge phenomena, which has promoted the understanding of gas discharge for investigators.

The existence of the floating conducting object in an air gap, would affect the electric field and discharge characteristics of the gap [13-15]. In [12], A discharge model containing floating conducting objects was put forward. In 1997, Kubuki [16] built experimental models of sphere-to-sphere gap and needle-plane gap containing floating metallic particles. The dc breakdown voltage was obtained experimentally and analytically. Furthermore, the breakdown performance of a rod-plane air gap containing a floating rod is analyzed experimentally in [17]. The measurement results showed that the minimum breakdown voltage emerges while floating rod is close to the high voltage electrode. These studies have focused mainly on the laboratory stage, while few concerns are mentioned on engineering applications.

The equipment in substations is compact. It is difficult to carry out live working in substations [18]. Considering the safety of operators and the increasing degree of automation, the measure of live working robots replacing manual maintenance has been popularized [19, 20]. While carrying out hot washing, live breaking lead wire, laser cleaning insulators [21] and so on, in these situations, there will be a robot with floating potential which is between the energized parts. As live working items are typically located several meters above the ground, metal materials can meet the mechanical requirements. In order to reduce the potential gradient and electromagnetic shield, robots are designed to be ungrounded. Therefore, robots are ungrounded and made of metal mostly. They may work near electrodes, thus floating conducting objects could be formed, constituting complex gaps.

Previous research attempts for the breakdown mechanism and model of complex gap. While little attention is paid to the size of live working robots. For the purpose of avoiding the breakdown of the phase-to-phase gap, the appropriate location and size of the robots would be of much concern. While carrying out live working, the auto-reclosing has to be laid off. Switching overvoltage is the main factor affecting security. Therefore, in this paper, the lowest discharge position and the critical size of live working robots were obtained under switching impulse. Based on Rizk's paper [11], a discharge model is applied, which contains a live working robot between 220 kV busbars.

2. Models and methods

Generally speaking, live working between busbars is a relatively risky item. There are two reasons for that. Firstly, the switching overvoltage in phase-

to-phase is more critical than phase-to-ground while live working. Secondly, the length of air insulation in phase-to-phase is strict than phase-to-ground. Therefore, supposing the live working robot working between two phases, the interphase air gap is divided into two different parts, which are defined as d_1 and d_2 respectively, shown in Fig. 1. The robot become a floating conducting object. The height of the busbar (h) to the ground is 9.45 m, and the distance between phase-to-phase is 3.25 m in 220 kV substation. The diameter of busbar is 0.175 m. The size of the live working robot (l_R) is shown in Fig. 1, too. Considering that the actual robot surface is inevitably irregularity, the protrusion is set according to the actual conditions. The length of the protrusion is l_p, and d_z is the distance from the center of the robot to the busbar. In addition, a complex gap is formed containing d_1 gap, floating robot and d_2 gap.

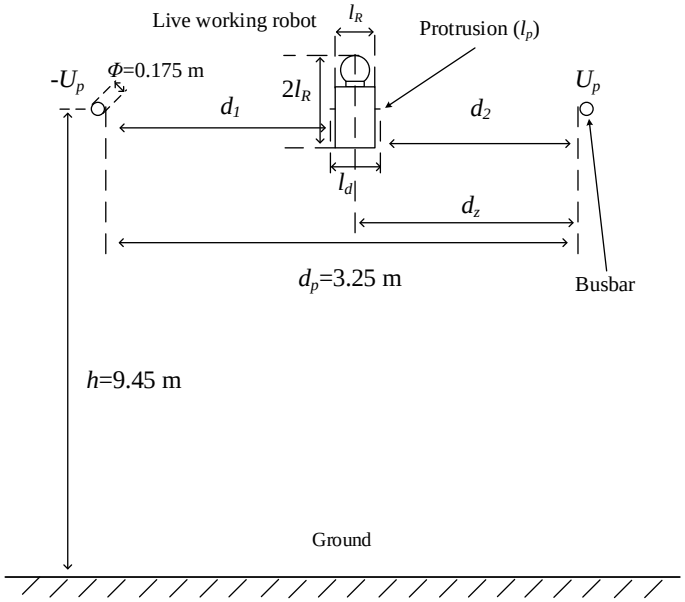

Fig. 1. Phase-to-phase configuration

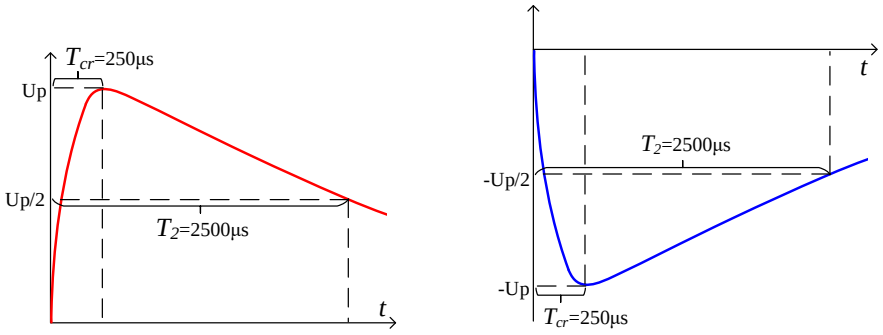

a. positive switching impulse b. negative switching impulse

Fig. 2. Standard switching impulse

In this model, the busbar on the right is applied positive switching impulse U_p while another one is negative impulse -U_p. Hence the peak voltage between the two busbars could reach 2U_p at the instant of T_{cr}. The standard switching impulse (250/2500 μs) is shown in Fig. 2. While studying the characteristics of gap discharge, it is important to solve the robot potential u_r, which can be calculated by the following expression (1):

$$u_r = u_e + u_i + u_f \tag{1}$$

where: u_e is the potential because of the electroquasistatic (EQS) field, which is related to spatial position of electrodes. u_i is the potential caused by a space charge, which could be confirmed while the position and magnitude of the space charges are clearly. u_f reflects the effect of the free charge gathering on the metal robot, which could be ignored because of the presence of the protrusion [12].

2.1 Streamer breakdown voltage

According to the streamer-leader breakdown theory [22], if the d_1 gap is narrow, it may be broken by streamer while leader has not yet developed. Under this circumstance, the streamer breakdown voltage U_{ps} can be judged by (2):

$$U_{ps} = u_e + E_s \cdot d_1 \tag{2}$$

where: u_e is mentioned in (1), and it can be calculated by finite element method. E_s is the streamer gradient, which can be chosen as 400 kV/m [23].

Defining a coefficient k_0:

$$u_e = k_0 U_{ps} \tag{3}$$

Equation (2) can be rewritten as (4):

$$U_{ps} = E_s \cdot d_1 / (1 - k_0) \tag{4}$$

Once d_1 gap is penetrated by streamer, leader inception starts to develop due to the self-capacitance of the floating conducting robot (see Fig. 2). The potential of the robot will have gone up to U_{rr} shown in (5):

$$U_{rr} = U_{ps} - \Delta U_{l1} \tag{5}$$

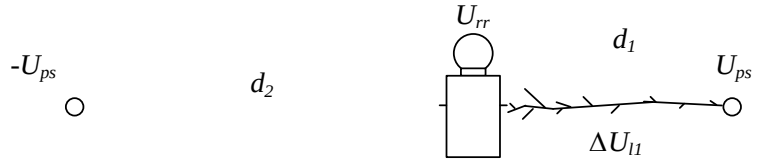

Fig. 3. d_1 gap is bridged by leader

Once the d_1 gap has broken down, for the d_2 gap, the streamer breakdown voltage U_{ps} can be calculated in (6):

$$U_{rr} - (-U_{ps}) = E_s \cdot d_2 \tag{6}$$

2.2 Leader inception and breakdown voltage

For relatively long air gaps, the streamer cannot penetrate the gap completely. When the streamer has developed to a certain extent, the leader will emerge. Between the two busbars, leader inception takes place as long as the voltage U_p comes up to U_{lcp} in (7) [10]:

$$U_{lcp}=\frac{U_{c\infty}}{\left(\beta_1 k+\beta_2\right)\left(1+\frac{A}{R_p}+0.25\left(\frac{\beta_2 k+\beta_1}{\beta_1 k+\beta_2}\right)^2\cdot\left(\frac{2}{d\ln\left(\frac{d}{a}\right)}-\frac{\ln\left(\frac{d}{a}\right)}{2h\ln\left(\frac{2h}{a}\right)\ln\left(\frac{2h}{\sqrt{ad}}\right)}\right)\right)} \tag{7}$$

where: the value of k is equal to an absolute value, which is the ratio of the voltage of the two busbars. The value of k is 1 in this model according to Fig. 1. h is the height of the busbar, a is the radius of the busbar, d is the length of air gap between busbars, which equals $d_1+d_2-l_R$. $U_{c\infty}$ can be taken as 2247 kV for a conductor-type [11]. β_1 and β_2 are geometric factors, R_p is a geometric function, A is a constant. The value of them is given in (8) to (10) according to [10]:

$$\beta_1=\frac{\ln\left(\frac{2h}{a}\right)\ln\left(\frac{\sqrt{d^2+4h^2}}{d}\right)}{\left(\ln\left(\frac{2h}{a}\right)\right)^2-\left(\ln\left(\frac{\sqrt{d^2+4h^2}}{d}\right)\right)^2} \tag{8}$$

$$\beta_2=\frac{\left(\ln\left(\frac{2h}{a}\right)\right)^2}{\left(\ln\left(\frac{2h}{a}\right)\right)^2-\left(\ln\left(\frac{\sqrt{d^2+4h^2}}{d}\right)\right)^2} \tag{9}$$

$$\frac{A}{R_p}=\left(5.15-5.49\ln a\right)\left(\frac{2\psi\left(\frac{a}{d}\right)}{d\ln\left(\frac{d}{a}\right)}+\frac{\ln\left(\frac{d}{a}\right)}{2h\ln\left(\frac{2h}{a}\right)\ln\left(\frac{2h}{\sqrt{ad}}\right)}\right) \tag{10}$$

The function ψ can be express by (11).

$$\psi\left(\frac{a}{d}\right)=\frac{2}{\pi}\int_0^{\infty}\frac{\left(B_0(n)\right)^2}{B_0\left(\frac{an}{d}\right)}\,dn \tag{11}$$

where: B_0 is the Bessel function after modified.

Before the gap is bridged by streamers, a final jump begins to develop. Supposing the length of the leader is d, the voltage decrease on it could be expressed by (12) [11].

$$\begin{cases} \Delta U_l = 50 l_z + 37.5 \ln\left(8 - 7e^{-1.33 l_z}\right) & (kV, m) \\ l_z = d - \dfrac{2U_{lcp}}{E_{sl}} \end{cases} \tag{12}$$

where: l_z is the leader length while final jump is developed.

Therefore, the breakdown voltage of relatively long gaps U_{pB} can be determined by (13) [11].

$$U_{pB} = U_{lc} + \Delta U_l \tag{13}$$

where: U_{lc} is the voltage of leader inception.

Considering that the voltages of the two busbars are of opposite polarity, the value of U_{pB} should be doubled while obtaining $U_{50\%}$. The 50% breakdown voltage $U_{50\%}$ can be obtained in (14).

$$U_{50\%} = \frac{2U_{pB}}{1 - 3\sigma} \tag{14}$$

where: σ is the standard deviation, which is taken as 3% in the paper.

2.3 Calculation of breakdown voltage of complex gap

In order to obtain the breakdown voltage and the characteristics of the complex gap, six parameters were given below. For comparison purposes, the values required for U_p at different stages are listed in Table 1.

Based on the six parameters, the scheme for obtaining the fifty percent disruptive discharge voltage ($U_{50\%}$) of complex gaps is shown in Fig. 4. In the beginning, determining the value of d_1 and l_R is the first step, which is essential for modeling. The second step is to figure out which gap would be penetrated first. If $U_p.\mathit{IV}$ is larger than $U_p.\ \mathit{I}$ and $U_p.\mathit{III}$, it means that breakdown occurs at d_1 gap first. Conversely, if any one of $U_p.\ \mathit{I}$ and $U_p.\mathit{III}$ is greater than $U_p.\mathit{IV}$, discharge may develop from d_2 gap. In the third step and fourth step, while d_2 gap gets breakdown first, if the voltage $U_p.\mathit{IV}$ that penetrates the d_2 gap is sufficient to breakdown the d_1 gap, the breakdown voltage of the complex gap U_{pB} could be equal to $U_p.\mathit{IV}$. Otherwise the breakdown voltage would be taken as the smaller of $U_p.\ \mathit{V}$ and $U_p.\ \mathit{VI}$. If d_1 gap gets breakdown first, a similar process of comparison can be used. Before the final step, U_{pB} has been calculated.

Table 1

The values required for U_p at different stages

U_p	Prerequisites	The type of required voltage	The mechanism of breakdown
$U_p.\ \mathit{I}$	--	d_1 gap gets breakdown first;	leader
$U_p.\ \mathit{II}$	d_1 gap was penetrated;	penetrating d_2 gap;	leader
$U_p.\mathit{III}$	--	d_1 gap gets breakdown first;	streamer

$U_p.IV$	--	d_2 gap gets breakdown first;	streamer
$U_p.V$	d_2 gap was penetrated;	penetrating d_1 gap;	streamer
$U_p.VI$	d_2 gap was penetrated;	penetrating d_1 gap;	leader

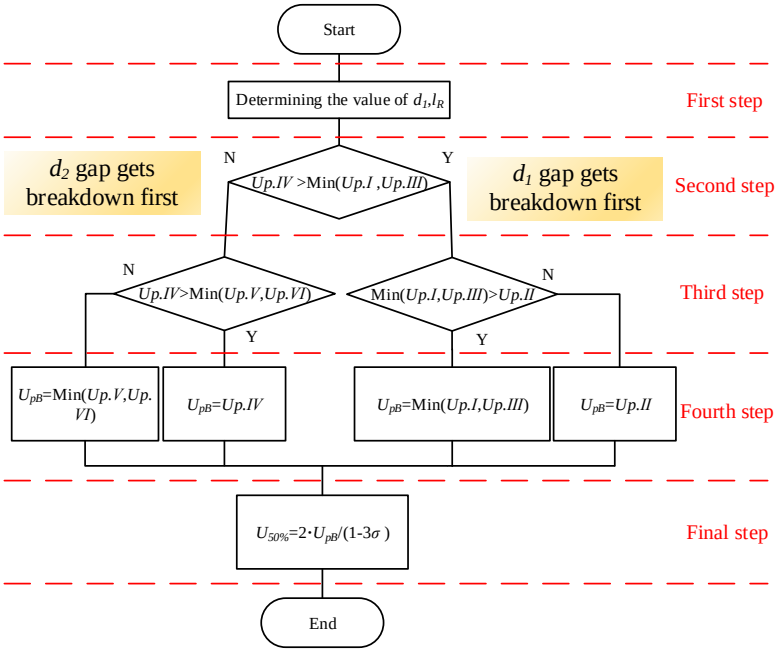

Fig. 4. Scheme for obtaining $U_{50\%}$ of complex gaps

2.4 Electroquasistatic field calculation

Before the calculation of the breakdown voltage, the electroquasistatic (EQS) field should be obtained. The value of u_e can be counted through the following equations.

$$\begin{cases} \nabla\cdot(\varepsilon E)=\rho \\ E=-\nabla V \\ J=\sigma E \end{cases} \tag{15}$$

where: E is the electric field strength. ε is the dielectric constant. σ is the electric conductivity. ρ is the charge density. J is the current density. Using finite element method (FEM) and (15), the electric field distribution could be drawn.

3. The lowest discharge position

In this section, the lowest discharge position is presented through electric field analysis and model calculation. Taking l_R for 0.2 m, the length of d_1 for 1.0

m and l_p for 0.02 m. According to the analysis of EQS field, k_0 is independent of U_p. Taking U_p for 800 kV, the potential distribution is shown in Fig. 5.

From the positive busbar to the negative busbar, the electric potential gradually decreases from +800 kV to -800 kV. Fig. 5 also includes the variation of the EQS field between the busbars. The potential of the inner part of the robot is a constant. Hence the inner electric field of the robot is close to zero. Near the negative busbar, the electric field strength is over 2500 kV/m. The maximum electric field of the robot occurs at the protrusion due to the small radius of curvature, which corresponds to the phenomenon that discharge develops in the vicinity of the protrusions.

The distance between the busbars is fixed as 3.25 m according to Fig. 2 and does not change. Table 1 shows values of k_0 corresponding to different length of the d_1 gap, which are calculated by (3). The value of k_0 tends to decrease gradually while the length of d_1 increases from 0.2 m to 2.8 m.

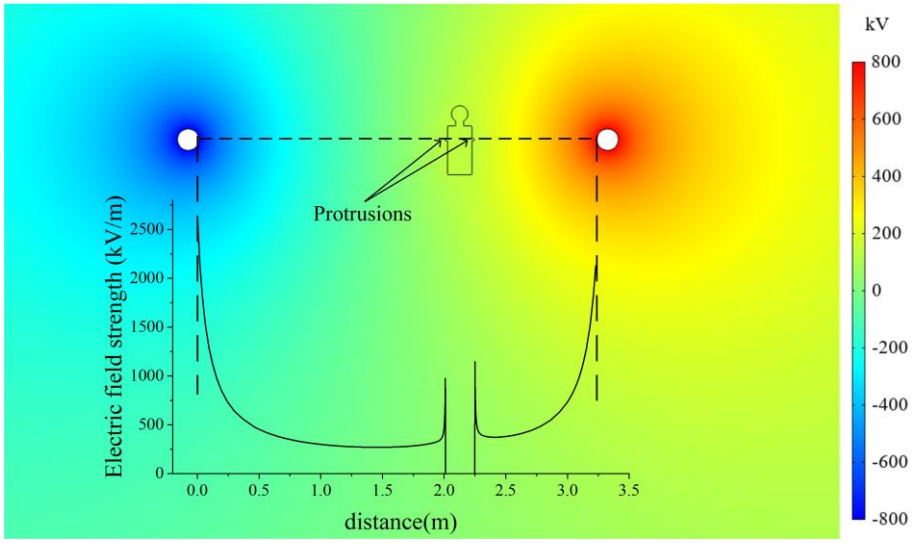

Fig. 5. Potential and electric filed strength distribution

Table 2

The value of k_0 for different lengths of d_1 gap

d_1/m	k_0	d_1/m	k_0
0.2	0.54912	1.6	-0.030237
0.4	0.41800	1.8	-0.09474
0.6	0.32012	2.0	-0.16199
0.8	0.23824	2.2	-0.23443
1.0	0.16546	2.4	-0.31573
1.2	0.09802	2.6	-0.41255
1.4	0.03343	2.8	-0.54113
1.5	0.00159		

Considering different values of d_1, the fifty percent disruptive discharge voltage ($U_{50\%}$) under switching impulse can be calculated. Fig. 6 shows the $U_{50\%}$ of the complex gap under different d_1. While d_1 is less than 1.5 m, d_1 gap may get penetrated first. Opposite results could be obtained when d_1 is greater than 1.6 m. Two troughs can be discovered in the curve, which correspond to d_1=1.2 m and d_1=2.0 m. Note that the lowest discharge position exists at d_1=2.0 m, which corresponds to 61.5% of the length of phase-to-phase gap d_p (see Fig. 1). The minimum $U_{50\%}$ amounts to 1059.5 kV. The maximum $U_{50\%}$ reaches 1543.9 kV when the live working robot is close to the negative busbar, which is 45.7% more than the minimum one.

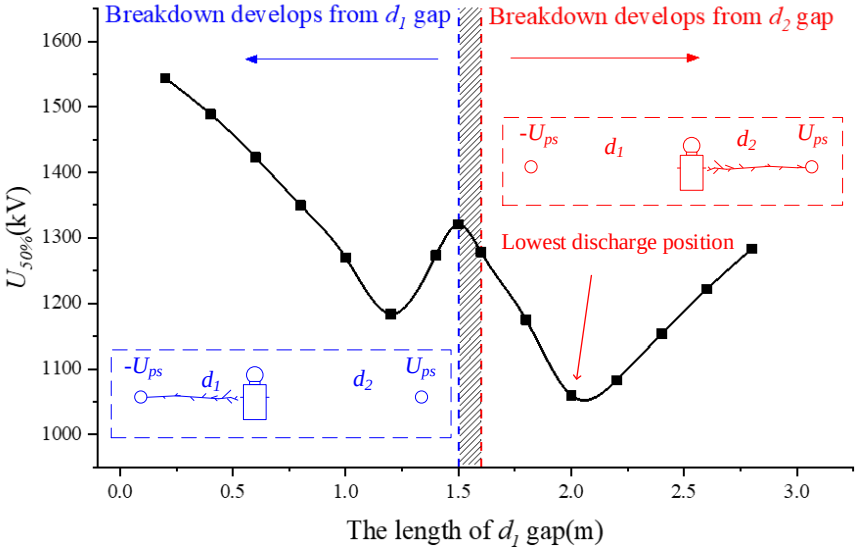

Fig. 6. The $U_{50\%}$ of the complex gap under different d_1

4. The critical robot size

In this section, to determine the critical size of the live working robot, the robot was located in the lowest discharge position. By changing the value of l_R, the corresponding discharge voltage can be obtained. Further, the 220 kV overvoltage level was combined. Consequently, the critical size of the live working robot may be confirmed.

Before the calculation of discharge voltage, k_0 has to be computed. In section 3, the lowest discharge position exists at d_1=2.0 m. In this case, d_z is equal to 1.13 m. In order to explore the effect of robot size, the center of the robot was kept at the lowest discharge position. Taking U_p for 800 kV, too. Fig. 7 illustrates the EQS field distribution when the robot is located in the lowest discharge position. Obviously, the electric field strength near the busbar is little affected by

the robot, which is over 2500 kV/m. The maximum electric field strength of the robot is distributed at the tip on the body surface.

Table 3 shows the value of k_0 for different robot size. One can appreciate from Table 2 that the value of k_0 changes very little as l_R increases from 0.1 m to 1.1 m. The values of k_0 are concentrated around -0.16. Thus it can be concluded that the value of k_0 is less related to l_R at the lowest discharge position.

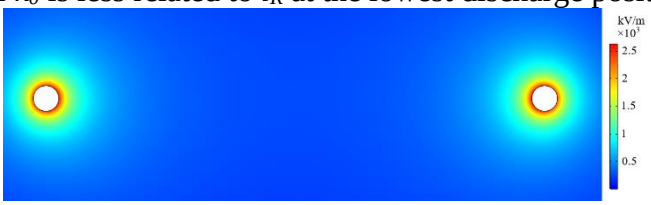

a. l_R=0 m

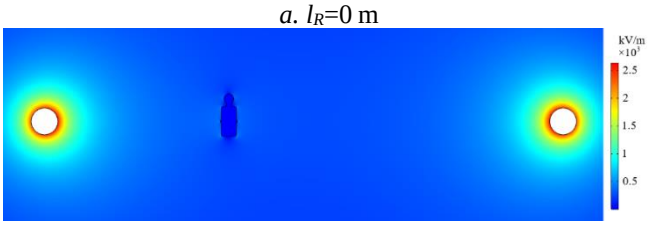

b. l_R=0.1 m

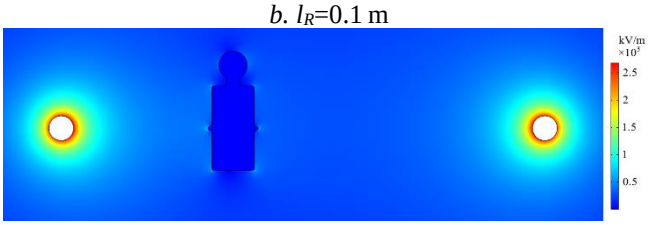

c. l_R=0.3 m

Fig. 7. Electric field distribution

Table 3

The value of k_0 for different robot size

l_R/m	k_0	l_R/m	k_0
0.1	-0.16220	0.7	-0.16059
0.2	-0.16199	0.8	-0.16154
0.3	-0.16150	0.9	-0.16331
0.4	-0.16093	1.0	-0.16612
0.5	-0.16046	1.1	-0.17023
0.6	-0.16028		

According to the National Standard, GB/T 19185: Calculation method of live working minimum approach distance on a.c. transmission line, the two percent statistical overvoltage between two phases ($U_{2\%}$) is:

$$U_{2\%} = \frac{\sqrt{2}}{\sqrt{3}} U_m k_p \tag{15}$$

where: U_m is the highest value of operating voltage. k_p is the statistical overvoltage phase to phase in per unit, which can be calculated by (16).

$$k_p = 1.33k_e + 0.4 \tag{16}$$

where: k_e is the per unit value of the two percent statistical overvoltage between two phases, which can be taken as 3.0 for 220 kV system according to GB/T 19185.

The value of $U_{2\%}$ is calculated to be 867.43 kV by (15) and (16), which is labelled in Fig. 8. Based on the calculation of k_0, The $U_{50\%}$ of the complex gap was represented in Fig. 8, too. It shows that the presence of the live working robot results in a sharp drop to the $U_{50\%}$ of the complex gap, from 1674.8 kV to 1101.8 kV. It is obvious that increasing the length of l_R limits the air gap considerably, which causes a decrease in $U_{50\%}$. The value of $U_{50\%}$ decreases as the length of l_R increases. While the value of l_R reaches 0.80 m, the corresponding $U_{50\%}$ is equal to 878.73 kV, which is a little higher than the value of $U_{2\%}$. Consequently, if the length of l_R exceeds 0.80m, the complex gap may be penetrated statistically.

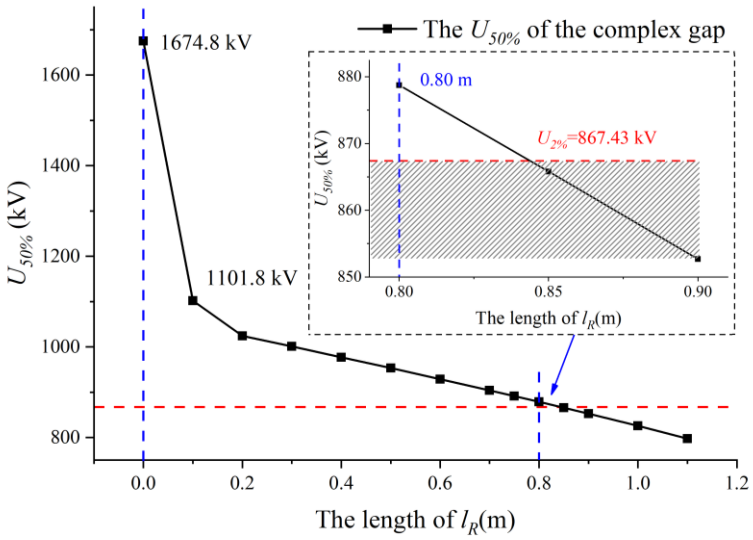

Fig. 8. The $U_{50\%}$ of the complex gap under different l_R

According to GB/T 19185, the risk of failure (R_0) is an important parameter which measures the safety of live working. The value of R_0 can be calculated through the following equations.

$$R_0 = \frac{1}{2}\int_0^{\infty} P_0(U)P_d(U)\mathrm{d}u \tag{17}$$

where: P_0 is the probability of density of overvoltage occurrence. P_d is the discharge probability of insulation.

$$P_0(U) = \frac{1}{\sigma_0\sqrt{2\pi}} \cdot e^{-\frac{1}{2}\left(\frac{U-U_a}{\sigma_0}\right)^2} \tag{18}$$

$$P_d(U) = \int_0^u \frac{1}{\sigma_d\sqrt{2\pi}} \cdot e^{-\frac{1}{2}\left(\frac{U-U_{50\%}}{\sigma_d}\right)^2} \mathrm{d}u \tag{19}$$

where: σ_d is the relative standard deviation which can be taken as 5%. U_a is the average value of operating overvoltage.

$$U_a = \frac{U_{2\%}}{1+2.05[\sigma_0]} \quad \text{(kV)} \tag{21}$$

where: $[\sigma_d]$ is taken as 12%.

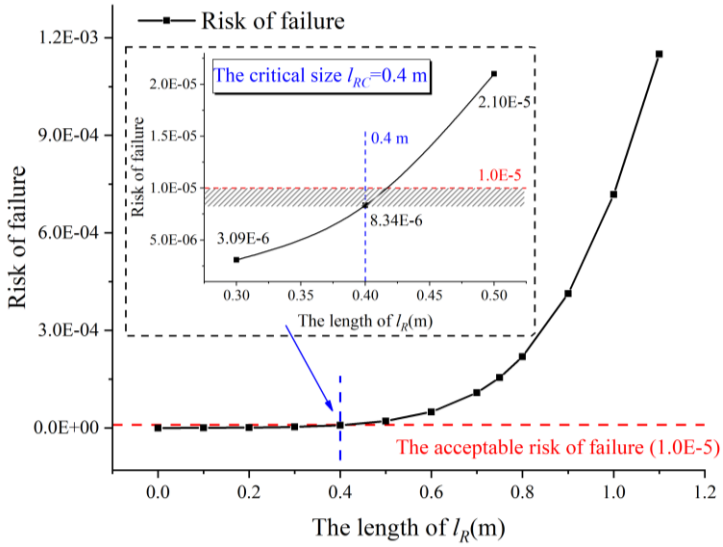

Fig. 9. The risk of failure (R_0) under different l_R

Fig. 9 shows the value of R_0 under different l_R. Generally, the acceptable R_0 is 1.0E-5, which is marked in Fig. 9, too. Observing Fig. 9, the value of R_0 increases monotonically with increasing l_R. That is to say, while the length of l_R is 0.4 m, R_0 is equal to 8.34E-6, which is little lower than the threshold (1.0E-5). Therefore, to ensure adequate safety while carrying out live working, the critical size of l_{RC} should be taken as 0.4 m.

5. Conclusions

In this paper, the breakdown voltage of complex gap containing a live working robot has been calculated. Further, the acceptable critical size of the live working robot is also explored.

While between the two busbars in 220 kV substations, the different positions that the robot located leads to different breakdown voltages of the complex gap. Breakdown develops from d_1 gap if the length of d_1 is less than 1.5 m. The lowest discharge position for the robot was pointed out, which was equal to 61.5% of the length of phase-to-phase gap. Moreover, the switching overvoltage and risk of failure was calculated to determine the critical size of the robot while carrying out live working. The presence of the live working robot results in a sharp drop in the $U_{50\%}$ and increasing the robot size leads to a

reduction in the $U_{50\%}$. To ensure the safety of the phase to phase complex gap in 220 kV substation while carrying out live working, the size of the live working robot l_R should be designed less than 0.4 m.

Acknowledgements

This research was funded by Guangdong Power Grid Co., Ltd. (Grant Number: 030700KK52180142).

R E F E R E N C E S

[1]. *Y. Fang, L. Wang, R. Li, Q. Zhang, J. Gao, and B. Song*, "A Modified Model for Discharge Voltage of AC Transmission Line-Tower Air Gaps", in IEEE Access. **vol. 7**, no. , May. 2019, pp. 71472-71480.

[2]. *L. Wang, Q. Zhang, J. Hu, K. Liu, T. Wu, and J. Wang*, "Research on complex gap discharge model of live working on EHV and UHV high-voltage transmission lines", in Canadian Journal of Electrical and Computer Engineering. **vol. 37**, no. 1, Apr. 2014 pp. 11-18.

[3]. *H. R. Armstrong and E. R. Whitehead*, "Field and Analytical Studies of Transmission Line Shielding", in IEEE Transactions on Power Apparatus and Systems. **vol. 87**, no. 1, Nov. 1968, pp. 270-281.

[4]. *G. W. Brown and E. R. Whitehead*, "Field and Analytical Studies of Transmission Line Shielding: Part || ", in IEEE Transactions on Power Apparatus and Systems. **vol. 88**, no. 5, May. 1969, pp. 617-626.

[5]. *I. Gallimberti*, "The mechanism of the long spark formation", in Journal de Physique Colloques. **vol. 7**, no. C7, Jan. 1979, pp. C7-193-C7-250.

[6]. *A. J. Eriksson*, "An Improved Electrogeometric Model for Transmission Line Shielding Analysis", in IEEE Transactions on Power Delivery. **vol. 2**; 2, no. 3, Jul. 1987, pp. 871-886.

[7]. *L. Dellera and E. Garbagnati*, "Lightning stroke simulation by means of the leader progression model. I. Description of the model and evaluation of exposure of free-standing structures", in IEEE Transactions on Power Delivery. **vol. 5**, no. 4, Apr. 1990, pp. 2009-2022.

[8]. *L. Dellera and E. Garbagnati*, "Lightning stroke simulation by means of the leader progression model. II. Exposure and shielding failure evaluation of overhead lines with assessment of application graphs", in IEEE Transactions on Power Delivery. **vol. 5**, no. 4, Apr. 1990, pp. 2023-2029.

[9]. *F. A. M. Rizk*, "Switching impulse strength of air insulation: leader inception criterion", in IEEE Transactions on Power Delivery. **vol. 4**, no. 4, Oct. 1989, pp. 2187-2195.

[10]. *F. A. M. Rizk*, "Critical switching impulse strength of phase-to-phase air insulation", in IEEE Transactions on Power Delivery. **vol. 8**, no. 3, Jul. 1993, pp. 1492-1506.

[11]. *F. A. M. Rizk*, "A model for switching impulse leader inception and breakdown of long air-gaps", in IEEE Transactions on Power Delivery. **vol. 4**, no. 1, Jan. 1989, pp. 596-606.

[12]. *F. A. M. Rizk*, "Effect of floating conducting objects on critical switching impulse breakdown of air insulation", in IEEE Transactions on Power Delivery. **vol. 10**, no. 3, Jul. 1995, pp. 1360-1370.

[13]. *M. Kubuki, R. Yoshimoto, K. Tanoue, and M. Hara*, "Breakdown characteristics in air gaps with artificial floating metals under DC voltage", in IEEE Transactions on Dielectrics and Electrical Insulation. **vol. 2**, no. 1, Feb. 1995, pp. 155-166.

[14]. *F. Roman, V. Cooray and V. Scuka*, "Comparison of the breakdown of rod-plane gaps with floating electrode", in IEEE Transactions on Dielectrics and Electrical Insulation. **vol. 5**, no. 4, Aug. 1998, pp. 622-624.

[15]. *T. Takuma and T. Kawamoto*, "Numerical calculation of electric fields with a floating conductor", in IEEE Transactions on Dielectrics and Electrical Insulation. **vol. 4**, no. 2, Apr. 1997, pp. 177-181.

[16]. *M. Kubuki, R. Yoshimoto, K. Yoshizumi, S. Tsuru, and M. Hara*, "Estimation of dc breakdown mechanisms in air gaps containing floating metallic particles", in IEEE Transactions on Dielectrics and Electrical Insulation. **vol. 4**, no. 1, Feb. 1997, pp. 92-101.

[17]. *G. Yang, S. Wang, W. Chen, F. Lv, B. Han, and X. Wang*, "Effect of a floating conductor on the breakdown performance of a rod–plane air gap", in The Journal of Engineering. **vol. 2019**, no. 16, Mar. 2019, pp. 3160-3163.

[18]. *B. Xiao, K. Liu, T. Wu, T. Liu, Y. Peng, X. Lei, Z. Su, and P. Tang*, "Experimental research on minimum approach distances and complex gaps for live working in substation", in Proceedings of 5th International Conference on Electric Utility Deregulation and Restructuring and Power Technologies, Changsha, China, Mar. 2016, pp. 1595-1599.

[19]. *X. Xiaopeng, X. Hongwei and Y. Ruqing*, "Control system design of high-voltage live cleaning robot based on security", in Journal of Systems Engineering and Electronics. **vol. 15**, no. 4, Dec. 2004, pp. 592-597.

[20]. *J. Li, J. Su, M. Fu, S. Lu, and X. Dong*, "Research and application of the Water Washing Robot with hot-line working used in 220kV open type substation", in Proceedings of 4th International Conference on Applied Robotics for the Power Industry, Jinan, China, Nov. 2016, pp. 1-5.

[21]. *J. Tian, X. Li, Z. Tang, C. Wu, W. Zhou, and A. Wang*, "Numerical Analysis on Surface Temperature of Polluted Porcelain Insulator by Laser Cleaning," in Proceedings of 5th Asia Conference on Power and Electrical Engineering, Chengdu, China, Jun. 2020, pp. 2154-2158.

[22] *U. Schubert, A. Shirvani, U. Schmidt, S. Kornhuber, and E. Kynast*, "Proposal for a General Atmospheric Correction Method of Breakdown and Withstand Voltages of Air-Gap Insulated Configurations Based on a Streamer–Leader Differentiated Model of the Breakdown Process", in Energies. **vol. 11**, no. 4, Mar. 2018, pp. 776.

[23] *G. Carrara and L. Thione*, "Switching surge strength of large air gaps: A physical approach", in IEEE Transactions on Power Apparatus and Systems. **vol. 95**, no. 2, Mar. 1976, pp. 512-524.